Transition from an optical precursor in coupled-resonator-induced transparency to coherent energy exchange in Autler-Townes splitting

Transition from an optical precursor in coupled-resonator-induced transparency to coherent energy exchange in Autler-Townes splitting

Tohru Oishi, Ryuta Suzuki, Aminul I. Talukder, and Makoto Tomita
Department of Physics, Faculty of Science, Shizuoka University, 836, Ohya, Suruga-ku, Shizuoka, 422-8529, Japan
(Received 11 June 2013; published 27 August 2013)

We investigated the transient responses of coupled optical resonators, after they were injected with square modulated temporal pulses. A sharp spike, attributed to the optical precursor in coupled-resonator-induced transparency, appeared when the coupling between the resonators was weak. As the coupling strength increased, the resonance spectrum developed clearly separated double dips of Autler-Townes splitting, and the precursor spike transformed into an oscillatory structure. These temporal oscillations were attributed to the coherent energy exchange between two resonators. Theoretical calculations were in good agreement with the experimental observations.

DOI: 10.1103/PhysRevA.88.023847 PACS number(s): 42.25.Bs, 42.50.Gy, 42.60.Da

I. INTRODUCTION

In recent years, there has been a discussion on the discrimination of two similar but different effects that both yield transparency in an absorption profile in the presence of a coupling field [1–3]. One is electromagnetically induced transparency (EIT), which arises from a quantum Fano interference between two paths and occurs even at very low control intensity. The other effect is Autler-Townes splitting (ATS) in a three-level atom, which appears as the dressed states in the excited level in the presence of a strong-coupling field. Because the differences between EIT and ATS are important in applications such as slow light, optical storage, and quantum information processing, different configurations of three-level atomic systems that feature EIT and/or ATS are studied in detail [3]. Recently, an objective method based on the Akaike information criterion was introduced to discriminate these two effects [1,2] and was successfully applied to experimental data in cold cesium atoms. Induced transparency has developed in various systems, such as those found in plasmons [4], metamaterials [5], and optical mechanical systems [6,7]. Particularly, in coupled-resonator-induced transparency (CRIT), two optical resonators of high and low Q values are coupled, and the destructive interference of the two optical pathways cancels the absorption [8–11].

Unique features of EIT and CRIT appear not only in the spectral domain, but also in the time domain. Recently, the advantages of using EIT and slow light were suggested for the observation of optical precursors [12,13]. That is, when a long square modulated laser pulse propagated through a cold atomic ensemble with EIT, transient spikes following the rising and falling edges appeared. These spikes are attributed to Sommerfeld and Brillouin precursors. Hence, it has demonstrated that precursors and the main signal can be observed separately in the temporal region, with amplitudes comparable to that of the incident step in EIT. Similarly the optical precursors were also demonstrated in CRIT [14]. Although the transition between EIT and ATS has been investigated in the spectral domain [1–3], the effect is also expected to appear in the time domain. Here, we investigated the transient responses of coupled optical resonators with the coupling strength, after they were injected with square modulated temporal pulses. The coupled resonator can be described in an analogical way as a Λ-type three-level atomic system [15]. Hence, a similar transition from CRIT to Autler-Townes-type splitting is also expected in this system [15]; i.e., the strong coupling between two resonators modulates the phase and splits the degenerated eigenmodes into two modes. With increasing coupling strength, we observed the transition in the time domain, i.e., the optical precursor in the CRIT regime transformed into coherent oscillation of the energy exchange between the resonators in the ATS regime.

The paper is organized as follows. Section II describes the theory of CRIT and ATS showing the details of CRIT to ATS transition analytically. Section III discusses the numerical simulation results on the basis of analytic calculation described in Sec. II. Experimental results are discussed in Sec. IV and compared with the results obtained from the numerical simulation in Sec. III. Section V introduces a dynamic-system example in support of our results and discussions. Finally, Sec. VI presents our conclusions.

II. CRIT AND ATS

Figure 1 shows a schematic diagram of the coupled resonators. The stationary input-output characteristics of the coupled resonators can be analyzed based on directional-coupling theory [16]. The electric field of the output light, normalized by the incident light electric field, is given as

$$E(\nu) = (1-\bar{\gamma}_1)^{1/2}\left[\frac{y_1 - x_1 R_2(\nu)\exp(i\phi_1)}{1 - x_1 y_1 R_2(\nu)\exp(i\phi_1)}\right],$$

where

$$R_2(\nu) = (1-\bar{\gamma}_2)^{1/2}\left[\frac{y_2 - x_2\exp(i\phi_2)}{1 - x_2 y_2\exp(i\phi_2)}\right]. \quad (1)$$

x_i $(0 \leqslant x_i \leqslant 1)$ and y_i $(0 \leqslant y_i \leqslant 1)$ are the loss and coupling parameters, respectively, with $i = 1,2$ for the first (R_1) and second (R_2) ring resonators. The loss (x_i) parameter represents the attenuation of the electromagnetic field amplitude after one round trip in the ring. The coupling parameter (y_i) represents the amplitude transmittance through the coupler. Here, $\bar{\gamma}_i$ represents the insertion loss at the couplers, and $\phi_i(\nu)$ is the phase shift in the circulation orbit in the ring resonator R_i. The resonance linewidth of individual ring resonator can be given as $\Gamma_i = 2(1 - x_i y_i)/\sqrt{x_i y_i}$, under a condition when

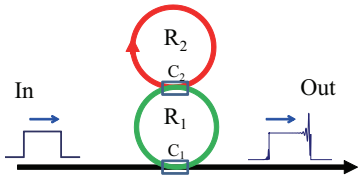

FIG. 1. (Color online) Schematic diagram of the experimental setup. R_1 and R_2 are ring resonators; C_1 and C_2 are couplers. Square modulated pulses were assumed as the input pulses.

two rings are decoupled. Equation (1) is an exposition of two distinct types of spectral lines, i.e., the spectral structures of CRIT and ATS depending on the coupling parameter y_2. To understand the transition between these two spectral features, we modify Eq. (1) with simplifications and approximations. First, we consider a situation, $\phi_1(\nu) = \phi_2(\nu)$, which indicates that both rings have the same cavity length. The internal loss in the second ring and the insertion losses broaden the resonance and only smear out the effect of the coupled resonators; hence we ignore these losses and set $x_2 = 1$, and $(1 - \bar{\gamma}_2)^{1/2} = 1$. For the first ring, we consider the critical coupling condition $x_1 = y_1$ as the typical case, which indicates the first ring is most efficiently coupled to the waveguide mode. The transmission of the coupled resonator shows an amplitude maximum at the off-resonance frequency $\phi = \pi$,

$$E_{\max} = \frac{y_1 + x_1 y_2 + y_1 x_2 y_2 + x_1 x_2}{1 + x_1 y_1 y_2 + x_2 y_2 + x_1 y_1 x_2}. \tag{2}$$

To extract the resonance effect in the spectral structure, we subtract the transmission electric field of Eq. (1) from $E_{\max}$,

$$\begin{aligned} E_{\max} - E(\phi) &= \frac{x_1(x_1^2 - 1)}{(x_1^2 + 1)} \frac{(e^{i2\phi} - 1)}{\{x_1^2(e^{i2\phi} - y_2 e^{i\phi}) + 1 - y_2 e^{i\phi}\}} \\ &= \frac{x_1(x_1^2 - 1)}{(x_1^2 + 1)} \left\{ \frac{A}{\phi - Z_1} + \frac{B}{\phi - Z_2} \right\}, \end{aligned} \tag{3}$$

where,

$$\begin{aligned} Z_1 &= i\gamma_c - \frac{\sqrt{\Lambda}}{2x_1^2}, \quad Z_2 = i\gamma_c + \frac{\sqrt{\Lambda}}{2x_1^2}, \\ \gamma_c &= 1 - \frac{y_2}{2}\left(1 + \frac{1}{x_1^2}\right), \\ \Lambda &= 4x_1^2 - y_2^2(x_1^2 + 1)^2, \end{aligned} \tag{4}$$

and

$$A = -\frac{2iZ_1}{Z_2 - Z_1}, \quad B = \frac{2iZ_2}{Z_2 - Z_1}. \tag{5}$$

Here the approximations $\exp(i\phi) \approx 1 + i\phi$ and $2i\phi - \phi^2 \approx 2i\phi$ are used, which are good as long as $\phi \ll 1$, i.e., the resonance linewidth is narrow compared to the free spectral range (FSR).

For the case of weak coupling, $\Lambda < 0$, i.e., for $y_2 > 2x_1/(x_1^2 + 1)$, the spectral poles of the amplitude transmittance in Eq. (3) are purely imaginary. Then, the absorption of the coupled resonator can be expressed as the difference between two Lorentzian line shapes,

$$E_{\max} - E(\phi) \propto \frac{A}{\phi - i\gamma_{\text{narrow}}} + \frac{B}{\phi - i\gamma_{\text{broad}}}, \tag{6}$$

where

$$\gamma_{\text{narrow}} = \gamma_c - \frac{\sqrt{|\Lambda|}}{2x_1^2}, \quad \gamma_{\text{broad}} = \gamma_c + \frac{\sqrt{|\Lambda|}}{2x_1^2}. \tag{7}$$

This indicates that the system is in the CRIT regime, where the spectral structure is expressed as the interference of two resonance profiles with γ_{narrow} and γ_{broad} centered at zero detuning frequency.

For the case of strong coupling, $\Lambda > 0$, i.e., for $y_2 < 2x_1/(x_1^2 + 1)$, the spectral poles of the transmittance are complex. Then, the absorption of the coupled resonator can be written as

$$E_{\max} - E(\phi) \propto \frac{A}{\phi - (\Omega_{\text{low}} + i\gamma_c)} + \frac{B}{\phi - (\Omega_{\text{high}} + i\gamma_c)}, \tag{8}$$

where

$$\Omega_{\text{low}} = -\frac{\sqrt{\Lambda}}{2x_1^2}, \quad \Omega_{\text{high}} = \frac{\sqrt{\Lambda}}{2x_1^2}. \tag{9}$$

This indicates that the system is in the ATS regime, where the spectral structure comprises two individual Lorentz lines at Ω_{low} and Ω_{high} with an equal linewidth of γ_c. The AT splitting represented by Eqs. (8) and (9) is $\Omega = \Omega_{\text{high}} - \Omega_{\text{low}} \propto \sqrt{1 - y_2^2}$ for the condition of $x_1 \to 1$.

III. SIMULATIONS

Although the analytical results show the transition from CRIT spectral structure to ATS, some simplifications and approximations are used in the calculation. To have a detailed picture about the transition, we numerically calculated the transmission spectra and transmitted pulse profiles using Fourier space analysis within the slowly varying approximation. The left column in Fig. 2 shows the theoretically calculated curves for the stationary transmission spectra through the coupled resonators. While various configurations of coupled resonator could be discussed, we assumed a fiber ring resonator in accordance with experiments described later. The coupling parameter, y_2, was decreased within the range of 1.0–0.95 (i.e., the coupling strength increased) in descending order from the top to the bottom graphs. Figure 2(a) shows the calculations for $y_2 = 1$; in this case, the second resonator has been decoupled, which means the system is converted into a single resonator, R_1. A broad dip with the width of $\gamma_1 = 5.3$ MHz (HWHM), appeared at the resonance frequency ν_1, in the transmission spectrum. Because the first resonator was set up under the critical coupling condition ($x_1 = y_1$), the stationary transmission was zero at $\delta\nu = 0$ in Fig. 2(a) [16]. The right column in Fig. 2 shows the theoretically calculated curves for the temporal profiles of transmitted pulses. We assumed square modulated pulses as the input pulse to study the transient response, following the traditional treatments by Sommerfeld and Brillouin. The incident pulse frequency was adjusted to the resonance frequency of the ring resonators at $\delta\nu = 0$. In contrast to the stationary transmission, when square modulated pulses were injected, the transient transmission was not zero; sharp spikes with comparable amplitude to the input pulses appeared at the leading and trailing edges of the pulses [Fig. 2(a′)]. These spikes were attributed to the

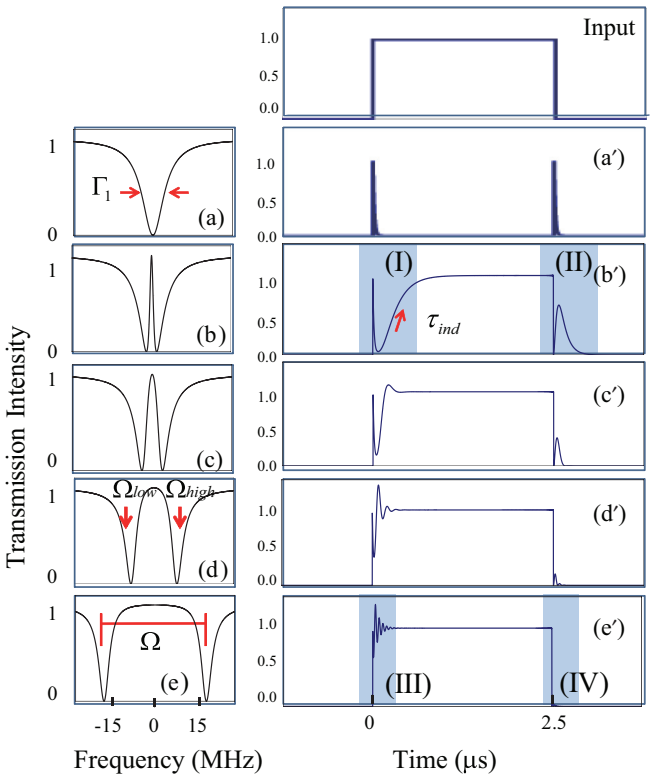

FIG. 2. (Color online) Left column; Theoretically calculated curves for the stationary transmission spectra. Right column: Transmitted temporal profiles of the square modulated pulses through the coupled resonator. The transmission intensity was normalized by the intensity of the input pulse. The parameters used were (a) (a′) $y_2 = 1.0$, (b) (b′) $y_2 = 0.9995$, (c) (c′) $y_2 = 0.998$, (d) (d′) $y_2 = 0.99$, and (e) (e′) $y_2 = 0.95$. Other parameters were $x_1 = 0.98$, $y_1 = 0.98$, $x_2 = 1$. $L_1 = 0.39$ m, $L_2 = 1.56$ m. The top graph in the right column represents the duration, 2.5 μs and a height of 1 for the square modulated input pulses. To visualize the precursors in the CRIT regime and oscillatory structures in the ATS regime clearly, the blue shaded areas noted (I)–(IV) are focused and projected in Fig. 3.

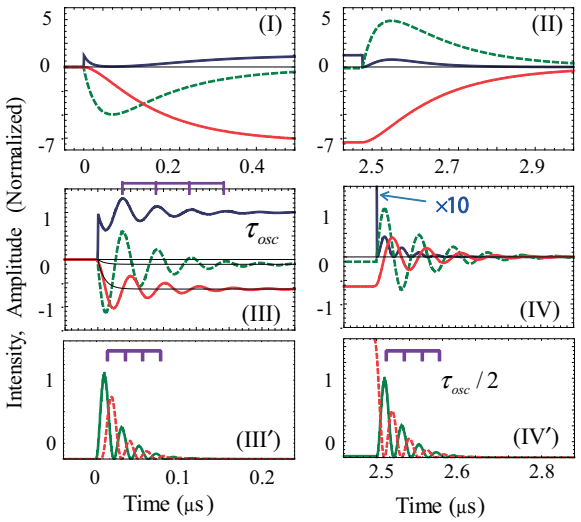

FIG. 3. (Color online) Detailed study of the shaded portions in Fig. 2. Here (I) and (II) are the expanded plots of blue shaded areas in Fig. 2(b′), for the weak-coupling condition, where CRIT is realized. The solid blue lines are transmitted intensity. The dashed green and dotted red lines are the electric field in the first and second ring resonators, respectively. The intensities and field amplitudes were normalized by those of the input pulse. Graphs (III) and (IV) are similar plots of the respective blue shaded areas in Fig. 2(e′), for the strong-coupling condition, where ATS is realized. The thin black lines in (III) are the averaged electric fields in the first and second ring resonators, respectively, where the oscillatory structures were removed. To show the oscillatory structures, transmitted intensity (solid blue line) was magnified by 10 × in (IV). The solid green and dashed red lines in (III′) and (IV′) are the oscillating energy portions in the first and second ring resonators, respectively. The comb in (III) represents the oscillation period in the amplitude basis. The combs in (III′) and (IV′) represent the period on intensity basis.

higher and lower spectral components of the square modulated pulse, consisting of sharp rising and falling edges to which the resonator did not respond; hence, they could be interpreted as optical pre- and postcursors [12–14,17]. The spikes occurred simultaneously as the square pulses entered the system and exhibited a decay of $\Gamma_1^{-1} = (2\gamma_1)^{-1} = Q_1/2\pi\nu_1$, where Q_1 is the Q value of the first cavity.

Figure 2(b) shows the calculated curves for the stationary transmission spectra when the second ring resonator is coupled to the first resonator, under the condition of $y_2 = 0.9995$. The second resonator modulated the loss and phase of the first resonator, and a narrow transparent window appeared at the resonance frequency of the second resonator, ν_2. This narrow transmission peak is caused by the destructive interference between two optical pathways: one passing through R_2 and another bypassing R_2; hence, we attribute this window to CRIT [8–11]. The linewidths of the first and the second rings were $\gamma_1 = 5.3$ MHz and $\gamma_2 = 0.03$ MHz, respectively, and the spectral splitting in Fig. 2(b) was $\Omega = 3.9$ MHz; thus a condition of $\Omega < \gamma_1 - \gamma_2$ had been satisfied. This indicated that the system was in the CRIT regime, where the spectral structure shown in Fig. 2(b) could be expressed as the interference of two resonance profiles of broad and narrow resonators centered at zero detuning frequency [3]. Note that this situation can be reinterpreted also as an overdamped condition, if we recognize the split broad resonance as two independent oscillations, because the splitting Ω is smaller than the linewidth Γ_1. As shown in Fig. 2(b′), when the square modulated pulses were injected into the coupled resonators, the main signals slowly increased according to the time constant, $\tau_{\rm ind} \sim \Gamma_2^{-1} = Q_2/2\pi\nu_2$, determined by the Q value of the second resonator R_2, after a sharp spike. This situation, therefore, demonstrates that the precursor and the main signal can be observed separately in the temporal regime, with amplitudes comparable to that of the incident square pulses [12–14]. In order to visualize the precursor structures in the CRIT regime clearly, the blue shaded areas (I) and (II) of Fig. 2(b′) are projected in Fig. 3 and discussed in detail in a separate paragraph.

To study the splitting as a function of coupling strength, the coupling parameter y_2 was further decreased to $y_2 = 0.998$, 0.99, and 0.95 in Figs. 2(c)–2(e), respectively. One can clearly see the development of well-separated double dips in the resonance spectra with increasing coupling strength. This situation can also be reinterpreted as an underdamped

condition. The spectral splitting was $\Omega = 8.5$, 17.3, and 38.6 MHz, in Figs. 2(c)–2(e), respectively, and agreed well with the expected value estimated from $\Omega \propto \sqrt{1 - y_2^2}$ [15]. The condition of $\Omega > \gamma_1 - \gamma_2$ was satisfied, indicating that the system was in the ATS regime of the underdamped configuration [3]. Figures 2(c′)–2(e′) show the transmitted pulse profiles. When a square modulated pulse is injected into the system in this configuration, the main signal shows no delay. Instead, we observe oscillatory structures in the leading and trailing edges of the pulse. These oscillatory structures that appeared in the ATS regime are shown clearly by focusing the blue shaded areas (III) and (IV) of Fig. 2(e′), and are discussed later in detail in Fig. 3.

To clarify the origin of the transient response, we calculated the electric fields inside the first and second resonators. Figures 3(I) and 3(II) show the internal field for the weak-coupling condition, $y_2 = 0.9995$, where CRIT is realized. As mentioned earlier, the time range for all plots in Figs. 3(I) and 3(II) correspond to that for blue shaded areas in (I) and (II) of Fig. 2(b′), respectively. The phase of the electric field shifts by $\pi/2$ every time it passes through the coupler. The electric field components having phase shifts of $\pi/2$ and π with respect to the incident fields are plotted for the first and the second resonators, respectively. In Fig. 3(I), when the input square pulse was turned on, the first resonator began to store the light energy (dashed green line), with a characteristic buildup time on the order of $\tau_1 \sim \Gamma_1^{-1}$. The circulated component from the first ring passed the coupler twice; hence, the phase was shifted π with respect to the direct component. The interference between the circulated and direct components resulted in zero stationary transmission. After the first resonator achieved this condition, the second ring resonator began to store the light energy with a characteristic buildup time on the order of $\tau_2 \sim \Gamma_2^{-1}$ (dotted red line). This component had the same phase as the direct component and appeared as a gradual increase of the main signal. It should be noted that the response time τ_2 explains the slow group delay time if Gaussian pulses propagate through the CRIT system. Figure 3(II) shows that the optical postcursor appeared after the exit of the square modulated pulses.

Figures 3(III) and 3(IV) now show the internal field for the strong-coupling condition, $y_2 = 0.95$, where ATS is realized. Similar to Figs. 3(I) and 3(II), the plotted time ranges of Figs. 3(III) and 3(IV) correspond to those of the blue shaded areas (III) and (IV) of Fig. 2(e′), respectively. In this case, the coupling strength was strong enough to cause the system to be in an underdamped configuration. The original resonator modes, ν_1 and ν_2, were no longer good eigenmodes; however, the reconfigured modes, Ω_{low} and Ω_{high}, i.e., the mixed modes of the first and second modes, provided a better description of the coupled system. As a result, the transmission intensity through the system (blue lines) exhibited an oscillatory structure. The averaged electric fields in the first and second ring resonators are plotted by the thin, solid black lines. To clearly show the energy exchange, the oscillating portions of the energy in the first and second ring resonators are plotted with solid green and dashed red lines in Figs. 3(III′) and 3(IV′), respectively, where the averaged electric field was subtracted and the energy density was summed over the total length of each resonator. It is clear from these plots that the two resonators reached the stationary state, exchanging mutual energies. The oscillation period was $\tau_{\text{osc}} = 51.8$ ns in Fig. 3(III′), which is in good agreement with $\tau_{\text{osc}} = 2/\Omega$. As the coupling parameter, y_2, decreased further, the spectral separation between the two dips increased and the oscillation period also decreased. The oscillation period of the postcursor in Fig. 3(IV) is also equal to τ_{osc}. The magnitude of the postcursor was weak, compared with that of the precursor. This difference in amplitude can be explained as follows. The precursor, at the leading edge, is detected as a heterodyne signal between the ballistic and circulated light. In contrast, the postcursor signal at the trailing edge is detected on an intensity basis, because there is no background ballistic field.

IV. EXPERIMENTS

Our simulations showed the transition from the optical precursor observed under weak-coupling conditions of CRIT to the oscillatory structure in the strong-coupling condition of ATS as the coupling strength increased. In simulation, the parameters can be changed continuously. The experimental system, however, had restrictions; we observed the transient response in two typical cases. The ring resonators were made using a single-mode polarization-maintaining (PM) fiber. The physical lengths of the rings were $L_1 = 1.8$ m and $L_2 = 3.6$ m. The main difficulty encountered in our experiment was the tuning of both resonators to a single resonance frequency. For this purpose, the fiber ring system was temperature controlled, within an accuracy of <1 mK. An Er-fiber laser at 1556 nm was used as the incident light source. The spectral width was 1 kHz, and the laser frequency was tuned by piezoelectric control of the cavity length. The laser frequency was scanned, and both the resonators of different lengths were found to oscillate at the same frequency. Square modulated pulses, with a temporal duration of $t_p = 2500$ ns and a repetition rate of 100 kHz, were generated using a $LiNbO_3$ (LN) modulator. The incident power of the pulses was 0.1 mW. The spectrum was observed in continuous-wave mode, where the LN modulator was operated in open mode. Transmitted intensity through the system was observed using a 1-GHz InGaAs photodetector and was recorded using a 600-MHz digital oscilloscope. For realization of the overdamped configuration [Fig. 4(b)], additional loss was inserted within the first resonator R_1. For realization of the underdamped configuration [Fig. 4(c)], it was important to minimize the internal loss. For this purpose, we used an InP/InGaAsP multi-quantum-well semiconductor optical amplifier within the first ring. Note that the semiconductor optical amplifier was operated at very low current to compensate for the intrinsic loss of the first ring, i.e., fiber loss and insertion loss of the couplers; the ring resonator was still the passive medium ($x_1 = 0.995$).

Figure 4(b) shows the experimental results when coupling strength between the two resonators is weak; hence, the system lies in the CRIT regime. The couplers were 60:40 ($y_1 = 0.78$) for C_1 and 90:10 ($y_2 = 0.95$) for C_2. The inset of Fig. 4(b) shows the transmission spectrum. The typical features of CRIT were observed; i.e., a transmission window was created, induced by the second resonator within the opaque spectral region, due to broad absorption by the first resonator. The widths of the first and the second (when decoupled) rings

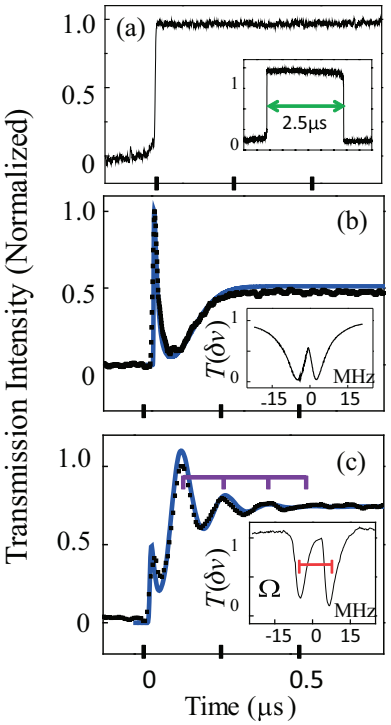

FIG. 4. (Color online) (a) Leading edge of the square modulated input pulses, where inset shows the overview of the pulses. (b) and (c) The transient response after the square modulated pulses were injected into the coupled resonators. The black dots represent experimental data, and the solid blue lines represent the fitted curves. The inset shows the transmission spectra as a function of laser detuning frequency. (b) Weak-coupling condition, where the system lies in the CRIT regime. The couplings, 60:40 ($y_1 = 0.78$) for the first coupler (C_1) and 90:10 ($y_2 = 0.95$) for second coupler (C_2), were used to achieve the overdamped configuration while the parameters used in the curve fitting were $x_1 = 0.8$, $y_1 = 0.775$, $x_2 = 0.975$, $y_2 = 0.94$. The sharp transient spike seen is attributed to the precursor. (c) Strong-coupling condition where the system lies in the ATS regime. The couplings, 60:40 ($y_1 = 0.78$) for C_1 and 70:30 ($y_2 = 0.83$) for C_2, were used to achieve the underdamped configuration while the parameters used in the curve fitting were $x_1 = 0.995$, $y_1 = 0.775$, $x_2 = 0.97$, $y_2 = 0.84$. The oscillatory structure is attributed to coherent energy exchange between two resonators.

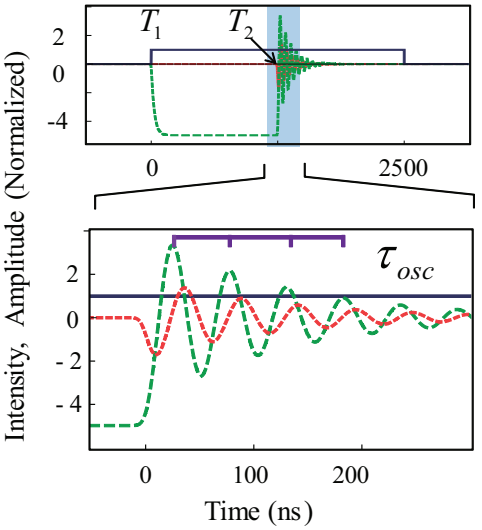

FIG. 5. (Color online) Electric fields inside the first and second resonators in the dynamically coupled resonator system. The lower graph is the expansion of the blue shaded area from the upper graph. The solid blue line represents the input intensity to the coupled resonator. The dashed green and dotted red lines are the electric fields in the first and second ring resonators, respectively, as a function of time. The parameters are time dependent; $y_1 = 0.9$ and $y_2 = 1.0$ (decoupled) for $t < T_2$, and $y_1 = 1.0$ (decoupled) and $y_2 = 0.95$ for $T_2 < t$. Other parameters are the same as in Fig. 2(e).

were $\gamma_1 = 14.9$ MHz and $\gamma_2 = 0.7$ MHz, respectively, and the splitting was $\Omega = 6.2$ MHz. The condition $\Omega < \gamma_1 - \gamma_2$ was satisfied, indicating that the system was in the CRIT regime. The main frame of Fig. 4(b) shows the transmitted pulse profiles at the leading edge of the square modulated pulses observed at the frequency of the induced transparency window. After the sharp spike, slow signals grew with a time constant determined by the second cavity, Γ_2^{-1}. The experimental observations were in good agreement with the calculation shown in Fig. 2(b′) in the CRIT condition.

Figure 4(c) shows the results when the coupling strength is strong; hence, the system lies in the ATS regime. The couplers were 60:40 ($y_1 = 0.78$) for C_1 and 70:30 ($y_2 = 0.83$) for C_2. In this case, the spectrum appears as well-separated double resonance dips of ATS. The spectral splitting was $\Omega = 11.8$ MHz and $\gamma_1 = 3.4$ MHz; thus a condition of $\Omega > \gamma_1 - \gamma_2$ was satisfied. When square modulated pulses are injected into this system, the main signal shows no delay. Instead, we observed distinctive characteristics of oscillatory structures in the leading edges of the pulses, in accordance with Figs. 2(d′) and 2(e′). The measured time period for the oscillation was $\tau_{osc} = 150$ ns, which was in good agreement with the value of $2/\Omega$ ($= 169$ ns). The envelope of the oscillation decayed with a time constant of $1/\Gamma_c$, where Γ_c is the spectral width of the separated dips of modes.

V. A DYNAMIC SYSTEM

Strictly speaking, the coupled resonators discussed above could be described as an open system; i.e., the input and output light continuously enters and escapes from the system, respectively. To examine the coherent energy exchange more clearly, we performed another simulation using a more dynamic situation. Here, the input port was initially open, while the second coupler between the two resonators was closed. When the input light was injected at time T_1, the first resonator began storing field energy and reached a stable energy level after period $\tau_1 \approx \Gamma_1^{-1}$. The input port was then suddenly closed, and simultaneously, the coupling between the two resonators was opened at time T_2. Figure 5 shows the simulated results for the electric fields in the first and second resonators. As mentioned earlier, the first and second resonators, individually, do not have corresponding eigenstates; however, the superposition of these modes provided the necessary eigenmodes. The energy of the first resonator was transferred to the second resonator and then returned to the first resonator, showing an oscillatory structure, similar to the one shown in Fig. 2. The oscillation

period τ_{osc} was the same as the open system shown in Fig. 2, indicating that the oscillation in Fig. 2 was due to the coherent energy exchange process between the two resonators.

VI. CONCLUSION

In summary, we observed the transition in time domain, from the optical precursor in the CRIT regime to coherent oscillation of energy exchange in the ATS regime, for a coupled resonator. While the objective method based on the Akaike information criterion clearly discriminates EIT and ATS in the frequency domain in Λ-type three-level atoms [1,2], the present observations indicate that the distinctive features also appear in the time domain. The effect discussed here could also be observed in atomic systems, as spike structures of the optical precursors and coherent transient responses have been observed in the atomic system [12,13,17].

ACKNOWLEDGMENT

The authors are grateful to Dr K. Totsuka for simulated discussions on the coherent energy exchanging effects.

[1] P. M. Anisimov, J. P. Dowling, and B. C. Sanders, Phys. Rev. Lett. **107**, 163604 (2011).
[2] L. Giner, L. Veissier, B. Sparkes, A. S. Sheremet, A. Nicolas, O. S. Mishina, M. Scherman, S. Burks, I. Shomroni, D. V. Kupriyanov, P. K. Lam, E. Giacobino, and J. Laurat, Phys. Rev. A **87**, 013823 (2013).
[3] T. Y. Abi-Salloum, Phys. Rev. A **81**, 053836 (2010).
[4] N. Liu, L. Langguth, T. Weiss, J. Kästel, M. Fleischhauer, T. Pfau, and H. Giessen, Nat. Mater. **8**, 758 (2009).
[5] N. Papasimakis, V. A. Fedotov, N. I. Zheludev, and S. L. Prosvirnin, Phys. Rev. Lett. **101**, 253903 (2008).
[6] S. Weis, R. Rivière, S. Deléglise, E. Gavartin, O. Arcizet, A. Schliesser, and T. J Kippenberg, Science **330**, 1520 (2010).
[7] Q. Lin, J. Rosenberg, D. Chang, R. Camacho, M. Eichenfield, K. J. Vahala, and O. Painter, Nat. Photonics **4**, 236 (2010).
[8] A. Naweed, G. Farca, S. I. Shopova, and A. T. Rosenberger, Phys. Rev. A **71**, 043804 (2005).
[9] Q. Xu, S. Sandhu, M. L. Povinelli, J. Shakya, S. Fan, and M. Lipson, Phys. Rev. Lett. **96**, 123901 (2006).
[10] K. Totsuka, N. Kobayashi, and M. Tomita, Phys. Rev. Lett. **98**, 213904 (2007).
[11] T. Oishi and M. Tomita, Phys. Rev. A **88**, 013813 (2013).
[12] D. Wei, J. F. Chen, M. M. T. Loy, G. K. L. Wong, and S. Du, Phys. Rev. Lett. **103**, 093602 (2009).
[13] J. F. Chen, S. Wang, D. Wei, M. M. T. Loy, G. K. L. Wong, and S. Du, Phys. Rev. A **81**, 033844 (2010).
[14] T. Oishi, R. Suzuki, P. Sultana, and M. Tomita, Opt. Lett. **37**, 2964 (2012).
[15] D. D. Smith, H. Chang, K. A. Fuller, A. T. Rosenberger, and R. W. Boyd, Phys. Rev. A **69**, 063804 (2004).
[16] K. Totsuka and M. Tomita, J. Opt. Soc. Am. B **23**, 2194 (2006).
[17] H. Jeong, A. M. C. Dawes, and D. J. Gauthier, Phys. Rev. Lett. **96**, 143901 (2006).